Korean J. Chem. Eng., 34(4), 1037-1043 (2017)
DOI: 10.1007/s11814-017-0008-2

pISSN: 0256-1115
eISSN: 1975-7220

Adsorptive removal of methylene blue from aqueous solution using different agricultural wastes as adsorbents

Sana Dardouri† and Jalila Sghaier

Unité de Recherche Thermique et Thermodynamique de Procédés Industriels,
Ecole National d'Ingénieurs Monastir, 5009, Tunisia
(*Received 3 March 2016 • accepted 2 February 2017*)

Abstract−The removal of dye from industrial wastewater is one of the most important subjects in water pollution regulation. Successive adsorption/desorption cycles of a basic dye, methylene blue, on internal almond shell, olive stone and rye straw were investigated by using fixed bed column experiments to study the adsorption capacity to remove the MB and adsorbents regeneration efficiency. The adsorption breakthrough curves were predicted by the Thomas model, Yoon Nelson model, and Wolborska model and modified dose-response model by using nonlinear regressive analysis. The adsorption capacity values obtained by this model are compared with the experimental capacity, noting an error of 16%, 27.8% and 18.9% for IAS, OS and RS respectively, but these errors are minimized in the second cycle to 22.98% and 6.06% for OS and RS respectively. The results show that the modified dose response model is more suitable for the description of breakthrough curves for three adsorbents only in the first cycle. The IAS presents the highest adsorption capacity and the best regeneration efficiency. Conversely, the RS presents lower adsorption capacity, whereas is not the hardest to regenerate.

Keywords: Fixed Bed Adsorption, Breakthrough Curves Modeling, Adsorbents Selection, Methylene Blue, Regeneration

INTRODUCTION

Water pollution has become a real threat due to rapid industrial development. The discharged wastewater of the textile industry, which contains persistent organic dyes, is one of the serious causes of water contamination. During dying and printing in the textile industry, a major fraction of dye disappears in the water, which makes the discharge colored. The main environmental problem in the textile industry is the treatment of liquid waste and its chemical loads. These dyes rejected by the industry represent a threat to the environment because of their low biodegradation and their high resistivity to classic purification treatment [1]. The presence of dyes in water is harmful for human health and the environment due to their toxic and mutagenic influence on human beings [2]. Several research studies have been devoted to the study of toxicity and mutagenic and carcinogenic effects of different types of dye on aquatic organisms (poison, algae, etc.). Among various commercial dyes, only basic dyes are toxic for algae [3]. These textile effluents are dramatic sources of pollution of ecosystems and aquatic life. They present a danger of bioaccumulation, which can affect humans by transport through the food chain.

Methylene blue (MB) is one of the most popular dyes used in textile industries and in the coloring of paper, wools, cotton, silk, etc [4]. MB has also been useful in medical applications. It is antiseptic against bacterial infection and is used as an antidote for cyanide poisoning [5]. Beyond its medical applications, the presence of MB in water threatens human health in various ways. Because of their high water solubility, dyes can move through rivers and affect the quality of water. MB as a cationic dye can readily interact with negatively charged surface cells and penetrate into the cells [6].

To reduce the negative effect of dyes, many proper treatments of wastewaters have recently attracted growing scientific attention. Various techniques have been applied for dye removal from wastewater such as adsorption [7-14], coagulation-flocculation, membrane filtration, chemical precipitation, ion exchange. Hence, many techniques for dye removal are proposed by incorporating physical, biological and chemical treatments. But because of the nonbiodegradable nature of many dyes [15], accordingly, the adsorption technique is the most suitable process and a more popular method for dye removal from aqueous solutions because adsorption has the advantages of high efficiency, flexibility, design simplicity, easy handling and economic feasibility. Many adsorbents are used for MB removal from aqueous solutions such as activated carbon [16], Clay [17], zeolite [18], sludge [19], almond gum [20], cashew nut shell [21], olive pomace [22], almond peel [23], and sawdust [24].

Olive stones, agricultural solid waste of the olive oil industry is abundant in large quantities in olive oil producing countries such as Tunisia, which has more than 60 million olive trees [25]. It was observed in batch studies and at basic pH that the maximum biosorption of MB dye in olive stone is equal to 13.2 mg/g [26].

Rye straw (RS) is an agricultural waste material which represents an abundant forestry residue and a low cost adsorbent. It can be used for removing pollutants from wastewater. In this work, rye straw as low cost adsorbent is reported for the removal of MB dye from aqueous solutions. There are only few researches focused on utilization of rye straw, in the adsorption of Cr (VI) [27] and in

†To whom correspondence should be addressed.
E-mail: sanadardouri_en@yahoo.fr

removal of azodyes [28].

Many studies have revealed that almond shells could be effectively used to remove dye from an aqueous solution [23,29]. Based on the analysis of process mechanisms involved in the sorption behavior of MB in almond shell confirms that the sorption process is particle-diffusion controlled [23]. It was found while using batch studies that the adsorption capacity of MB with initial concentration of 100 mgL^{-1} is equal experimentally and numerically to 52.35 mgg^{-1} and 54 mgg^{-1} respectively.

Several low-cost adsorbents are reported for the removal of heavy metals, agricultural waste such as olive stones, peach stones, almonds shell [29] and sheep manure waste [30]. In this work, almond shell (AS), which is available in abundance in Tunisia, was chosen as adsorbent for the removal of methylene blue.

In this research study, adsorption/desorption of MB on almond shell, olive stone and rye straw in a fixed bed column was investigated with the objective to (i) evaluate the adsorption capacity of adsorbents, (ii) predict a breakthrough curve model, and (iii) evaluate the removal efficiency and the regenerability of three adsorbents.

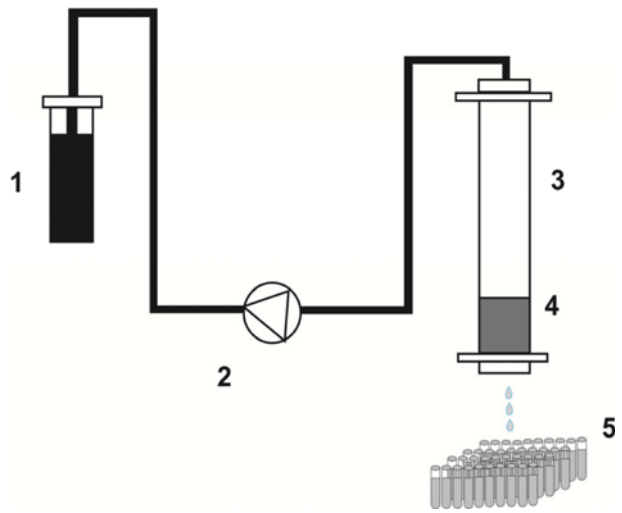

Fig. 1. Schematic of column setup.

1. Influent tank
2. Peristaltic pump
3. Column
4. Adsorbent
5. Effluent collection

MATERIALS AND METHODS

1. Materials

As low adsorbents, three materials have been used in the removal of MB from aqueous solutions: internal almond shell (IAS), olive stone (OS) and rye straw (RS). These wastes were collected from the region of Sousse in Tunisia. They were used directly for adsorption experiments without any treatment. The other adsorbents were dried in the air and crushed to a fine powder. The water infiltration versus time for all adsorbents was measured using mini disk infiltrometer (DECAGON Model S). The particle size distribution of three adsorbents was measured by laser diffraction particle size analyzer (Microtrac S3500).

The methylene blue used as adsorbate (basic blue 9, CI 52015) is a cationic dye with a molecular formula $C_{16}H_{18}ClN_3S{\cdot}3H_2O$ and a molar mass of 373.9 $gmol^{-1}$. The wavelength of maximum absorbance for MB is 663 nm.

2. Fixed Bed Column Sorption Experiments

The adsorption experiments were conducted using a glass column with an internal diameter of 3.25 cm and a height of 25 cm. The column was packed with the materials-bed length of 5 cm. The MB solution with inlet concentration of 100 mgL^{-1} was pumped at the top of the column using a peristaltic pump (ROTH CYCLO I) at a constant volumetric flow rate of 4 ml/min. Samples were collected and analyzed by spectrophotometer UV-visible (HACH LANGE DR3900).

3. Column Desorption and Recycling

To evaluate the feasibility of adsorbents for practical use and its reusability, the regeneration of these adsorbents was carried out through adsorption-desorption cycle. After adsorption had taken place, the adsorbed dye was eluted using water at a flow rate of 4 ml min^{-1}. The samples of the effluent were analyzed and all experiments were in duplicate. After the elution time, the adsorbent was reused in a second cycle for adsorption at the same conditions than the first cycle to study the reuse of the adsorbent.

RESULTS AND DISCUSSIONS

1. Breakthrough Curves and Analysis of Mass Transfer Zone

As shown in the obtained breakthrough curves (Fig. 3), the breakthrough time increases in order RS<OS<IAS (Table 1). It was observed that the breakthrough time of MB in OS and IAS was 108

Table 1. Adsorption capacity (q_s), Fraction capacity (FC) and Height of mass transfer zone (H_{MTZ}) for different adsorbents

	q_{ex} (mg/g)	FC	H_{ZTM} (cm)	t_{bk} (min)	V_{eff} (ml)	m (g)
IAS						
Cycle1	505.4	0.89	2.98	904	6672	37.88
Cycle2	477.8	0.84	5	1695	6780	37.88
OS						
Cycle1	101.67	0.855	4.85	613.8	2888	37.88
Cycle2	143.25	0.852	5	954.6	3820	37.88
RS						
Cycle1	180.04	0.72	4.24	252	1140	6.72
Cycle2	216.65	0.565	5	385.8	1544	6.72

min and 764 min respectively. However, compared with that in RS, the breakthrough time was 33 min. The breakthrough curve of IAS is very steep. This result affirms that the adsorption capacity of MB in IAS was significantly important and indicates that the mass transfer coefficient decreased from RS to OS.

Besides, the concentration gradients in batch systems are dissimilar from that of a continuous flow system [31]; the experimental results obtained using the batch systems appear difficult to apply to the processing of large volumes of water [32]. Continuous adsorption experiments are mostly used in several applications in chemical engineering, mainly in the adsorption of the components of a fluid flowing through a bed of a porous adsorbent material. This adsorption process on porous solids can be divided in four stages: (a) Transport of the adsorbate from the bulk of the solution to the exterior film encircling the adsorbent material (outer diffusion), (b) Movement of the adsorbate through the external liquid film boundary layer to external surface sites of adsorbents, (c) Migration of the adsorbate particles within the pores of the porous adsorbent by intraparticle diffusion (inter diffusion), and (d) Sorption of adsorbate at inner and outer surfaces of the adsorbent [33].

To provide more information about the adsorption process, we determined the quantities of MB retained in the bed until the exhaustion time (q_{ex}), the height of the mass transfer zone (H_{MTZ}), the fractional capacity (FC) and the percentage of saturation of the column (S).

The adsorption capacity at an exhaustion time (q_{ex}) is calculated according the Geankoplis model [34]:

$$q_{ex} = \frac{C_0 U}{m} \int_0^{t_{ex}} \left(1 - \frac{C_t}{C_0}\right) dt \quad (1)$$

where C_t and C_0 are the MB effluent and inlet concentration (mgL^{-1}); U is the flow rate ($mLmin^{-1}$), m is the mass of adsorbent (g) and t_{ex} is the exhaustion time (min). The fractional capacity represents the quantity of MB eliminated compared to the elimination capacity f adsorbent n the mass transfer zone:

$$FC = \frac{\int_{t_{bk}}^{t_{ex}} (C_0 - C_t) dt}{C_0 (t_{ex} - t_{bk})} \quad (2)$$

Eq. (3) represents the mass transfer zone, which is the total height of the adsorbent progressively being saturated:

$$H_{MTZ} = \frac{H(t_{ex} - t_{bk})}{t_{bk} + FC(t_{ex} - t_{bk})} \quad (3)$$

where H_{MTZ} is the height of the mass transfer zone (cm); H is the height of the fixed bed (cm), t_{ex} is the exhaustion time (min); t_b is the breakthrough time (min) and FC s the fractional capacity.

The percentage of saturation of bed column is calculated according to:

$$S(\%) = \frac{H + (FC - 1)H_{MTZ}}{H} * 100 \quad (4)$$

The adsorption capacities at exhaustion time (q_{ex}) follow the order OS<RS<IAS, which proves the results concluded from the breakthrough curves in Fig. 3. The difference in the shapes of the breakthrough curves for three adsorbents can be explained by the

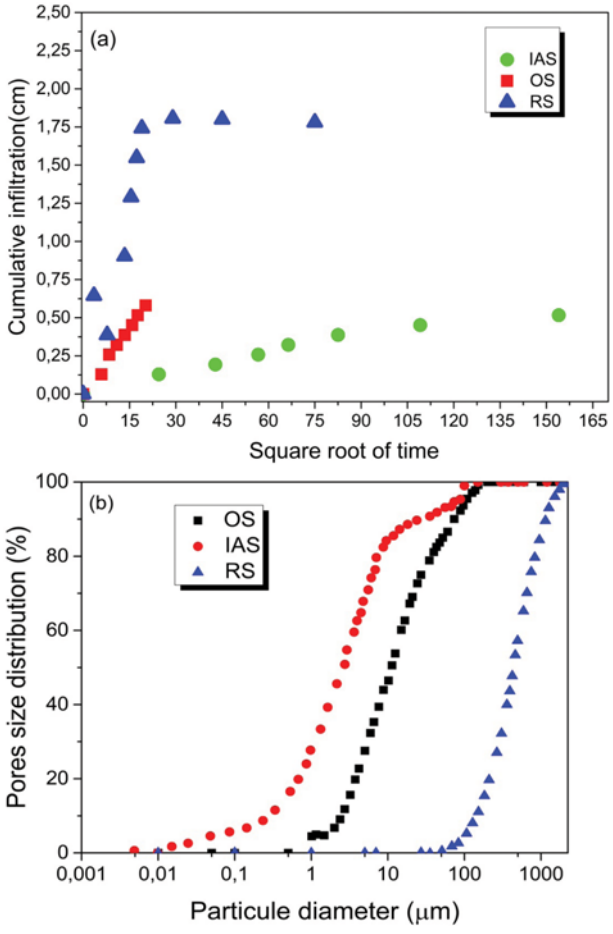

Fig. 2. (a) Cumulative water infiltration versus square root of time for IAS, OS and RS, (b) Particle size of three adsorbents.

internal diffusion of MB from the bulk liquid to the mesopores and then the micro pores, which causes slower adsorption kinetics [30]. However, the more the particle size decreases (Fig. 2(b)), the more the influence of the external film external mass transfer on the sorption becomes much more significant. The IAS is the

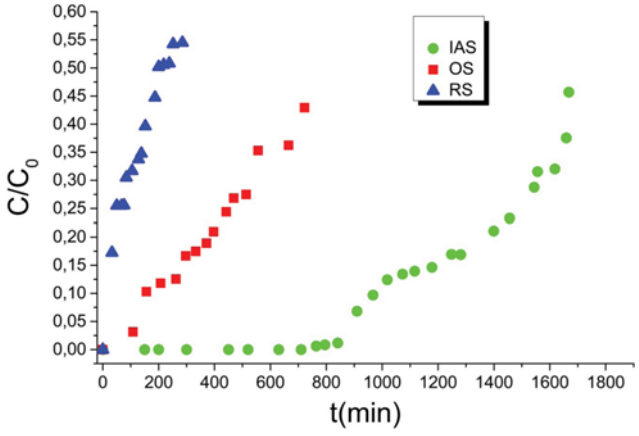

Fig. 3. Breakthrough curves representing MB adsorption onto IAS (circles), OS (squares) and RS (triangles).

Table 2. Predicted parameters for, Thomas, Yoon-Nelson, and Wolborska and Modified-dose response models for MB adsorption on IAS, SMW and sawdust materials

Model		IAS		OS		RS	
		Cycle1	Cycle2	Cycle1	Cycle2	Cycle1	Cycle2
Thomas	Kth *10^4 (L/minmg)	0.305	0.067	0.358	0.391	0.742	0.698
	q_0 (mg/g)	602.22	1125	140.5	186	218.7	230.6
	R^2	0.958	0.777	0.944	0.922	0.879	0.939
Yoon Nelson	K_{YN}*10^2 (min^{-1})	0.3	0.06	0.215	0.23	0.445	0.419
	ζ (min)	1806	3375	780	1032	222.6	235.2
	R^2	0.958	0.777	0.944	0.922	0.879	0.939
Wolborska	A	4.98	2.35	2.649	3.63	1.674	1.53
	B*10^2	0. 245	0.055	0. 25	0.283	0. 007	0.33
	R^2	0.955	0.773	0.917	0.935	0.829	0.859
MDR	a	3.84	0.42	1.46	3.11	0.86	1.17
	b	126.2	2277	61.98	70.77	15.41	13.89
	R^2	**0.96**	**0.82**	**0.97**	0.864	**0.972**	**0.97**

most micro porous material compared to RS and OS, which explains the tailing in the breakthrough curve (Fig. 3). The particle size of materials and its infiltration kinetics are related and have the same effect on adsorption capacity of the material. Indeed, large pores make greater contribution to transfer water in porous media than small pores, which are filled. This small pore entraps water flow as liquid is transported through weakly conductive pore medium, and it is accessed in the form of films to solid particle. As the infiltration kinetics increases, the ability of a material to transfer water and solute increases. The IAS has the lower infiltration rate (Fig. 2) and inhibits the water to infiltrate in its porous space, which makes more contact time between adsorbate and solid surface of IAS. This high residence time can explain the length of breakthrough time (t_{bk}=764 min).

During the dynamic contact of solid and liquid in bed column, the length and shape of the mass transfer zone (MTZ) provides insight about the performance of fixed bed columns. The area where the relative adsorbate concentration changes from 0.05 to 0.95 represents the region of MTZ where sorption practically takes place in fixed beds [35]. The shape of the curve is used to determine the height of the mass transfer zone. If this height is small, this indicates the existence of faster kinetics and lower diffusion resistance in the sorption process. The height of MTZ value increases as IAS<RS<OS (Table 1), thereby, the mass transfer efficiency has the opposite order, where IAS has the highest value. The same note goes for fractional capacity.

2. The Breakthrough Curves Modeling

To better describe the fixed bed column and to predict the MB breakthrough, many models are used to fit the experimental data. The breakthrough curves are analyzed using four of these modes: Thomas model, Yoon Nelson model, Wolborska model and modified-dose response model.

2-1. Thomas Model

The Thomas model assumes that a Langmuir isotherm and second-order kinetic fitted well the experimental data. It was assumed also that adsorption is limited by mass transfer with no axial dispersion is derived with adsorption. It allows the calculation of the adsorption rate constant. The equation of the Thomas model can be described as:

$$\frac{C_t}{C_0}=\frac{1}{1+\exp\left((q_0 m - C_0 \vartheta t)\frac{k_{th}}{\vartheta}\right)} \quad (5)$$

where k_{th} is Thomas rate constant (mL $min^{-1}mg^{-1}$), q_0 is equilibrium adsorption capacity (mgg^{-1}), m is the mass of the adsorbent, C_0 and C_t are the MB concentration in the influent and at time t (mgL^{-1}) and υ is the flow rate (mL min^{-1}).

The values of k_{th} and q_0 are determined using nonlinear fitting and shown in Table 2. The correlation coefficient (R^2) values ranged from 0.77 to 0.97 and were higher for OS. The adsorption capacity values obtained by this model were compared with the experimental capacity, noting an error of 16%, 27.8% and 18.9% for IAS, OS and RS, respectively, but these errors were minimized in the second cycle to 22.98% and 6.06% for OS and RS, respectively.

2-2. Yoon Nelson Model

The Yoon-Nelson model assumes that the rate of decrease in the probability of adsorption for each adsorbate molecule depends on the probability of adsorbate adsorption and the probability of an adsorbate breakthrough on the adsorbent [36]. The model can be expressed by Eq. (6):

$$\frac{C_t}{C_0}=\frac{1}{1+e^{(-k_{YN}(t-\tau))}} \quad (6)$$

where k_{YN} is the Yoon Nelson rate constant (min^{-1}) and τ s the time required for reach 50% adsorbate breakthrough (min).

The Yoon Nelson model is mathematically similar to the Thomas model as noted above. Therefore, the fitting results as shown in Table 2 were also good enough. For RS, the theoretical and experimental time required for 50% of adsorbate breakthrough correspond accurately (average percentage errors <10%).

2-3. Wolborska Model

The Wolborska model [37] is based on the application of equations of mass transfer for diffusion mechanisms used for the low concentration breakthrough curve. A simplified version is given by:

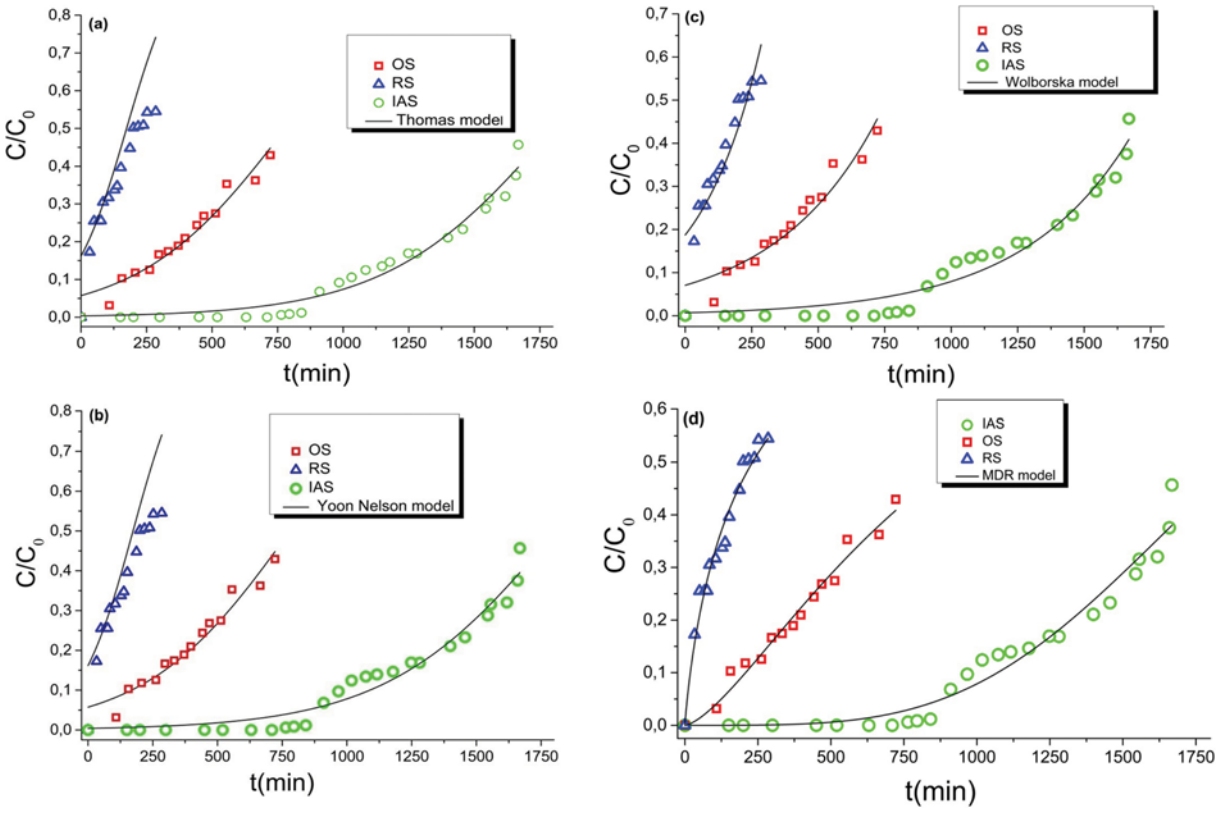

Fig. 4. Experimental and predicted breakthrough curves for MB removal based on Thomas model (a), Yoon-Nelson model (b), Wolborska model (c) and Modified-dose response model (d) for adsorption of MB onto IAS (circles), OS (squares) and RS (triangles).

$$\frac{C_t}{C_0}=\exp\left(\frac{\beta C_0}{N_0}t-\frac{\beta Z}{U}\right)=\exp(Bt-A) \quad (7)$$

where β is the kinetic coefficient of the external mass transfer (h^{-1}), N_0 is the exchange capacity (mgL^{-1}), $B=\beta C_0/N_0$; $A=\beta Z/U$.

This model is applied in the description of the breakthrough curve in the range of low concentration. The values of the Wolborska model parameters for three adsorbents are presented in Table 2. For sawdust, compared to Thomas model and Yoon Nelson model, the Wolborska model is the poorest and does not fit the breakthrough curve acceptably, especially in the first region of BTC. For RS in both cycles compared to Thomas model, the Wolborska model is the poorest and does not fit the breakthrough curve acceptably especially in the first region of BTC. The Wolborska model is valid only for OS in the second cycle.

2-4. Modified-dose Response Model

The modified-dose response model is also used to predict the breakthrough behavior in column adsorption. Mainly at lower or higher time periods of the breakthrough curve, the use of this model reduces the error resulting from the use of the Thomas model. The model equation is expressed as:

$$\frac{C_t}{C_0}=1-\frac{1}{1+(\upsilon t/b)^a} \quad (8)$$

where a and b are both the constant of the modified-dose response model.

Modified dose-response model was also used to fit the experimental data; the parameters of this model are also shown in Table 3. The values of R^2 from modified dose-response (0.96-0.97) were larger than those from other models in the first cycle. Comparing the fitted curves (Fig. 4) from the used models at the same condition, the fitted curve from modified dose-response model is closer to experimental curves.

For the models used to describe the experimental data, modified dose-response model fitted the data from column experiments significantly better than other model for the first cycle, while in second cycle this model was the weakest model in the fitting of

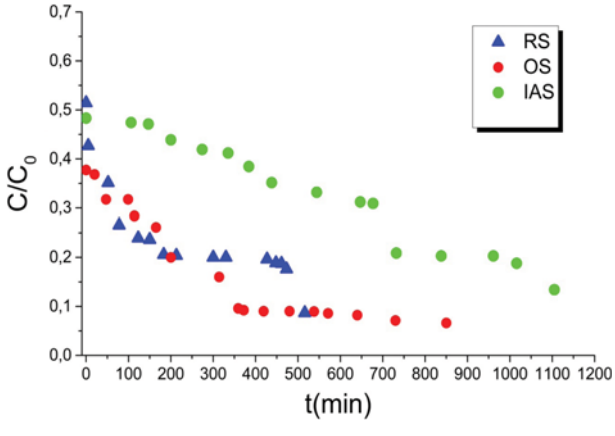

Fig. 5. Elution curve for MB desorption from the IAS (circles), SMW (squares) and Sawdust (triangles) fixed-beds.

experimental data of OS. Thus, the modified dose-response was applied specially in the first part of the breakthrough curve.

3. Column Regeneration

A potential and an effective adsorbent for dye removal must have a good adsorption capacity and have also a good desorption of dye. That is why it is necessary to investigate the desorption of MB from IAS, OS and RS.

The elution curve showed an asymmetric shape for three adsorbents (Fig. 5), which has a strong decrease at first tracking by a light decrease. The wide decrease is marked for RS with an effluent concentration of 0.51 C/C_0 at the initial time; therefore, the first part of adsorption curve represents the majority of MB amount desorbed from the bed. Unlike, IAS and OS have the maximum equal to 0.48 C_0 and 0.37 C_0, respectively, and only OS reached a negligible effluent concentration. As shown in Fig. 5, the elution curve demonstrates that RS, IAS and OS need longer desorption time to reach low concentration and achieve null values. The desorption efficiency of three materials follows the order SMW<OS< RS. After desorption studies, two cycles of adsorption were carried out, and the breakthrough curves obtained for the adsorption desorption cycles are shown in Fig. 6. The breakthrough curves for the first and second cycle have practically the same shape. A significant decrease of the breakthrough time (t_{bk}) is observed from the first to the second cycle with reduction of the amount of MB sorbed per unit mass of adsorbent in the column. The decrease of breakthrough time can be caused by the losses of dye particles during the elution step. The reduction of saturation of the bed column was from the first to the second cycle (Table 1), and the decrease of residence time was caused by the increase of the external film mass resistance at the surface of the adsorbents, resulting in a lower removal efficiency (Fig. 7(a)) [38].

Contrary to desorption efficiency, the regeneration efficiency increased as OS<RS<IAS (Fig. 7(b)). The worst regeneration efficiency was obtained with OS despite its high adsorption capacity compared to RS, due to the difficulty of desorbing from the micropores.

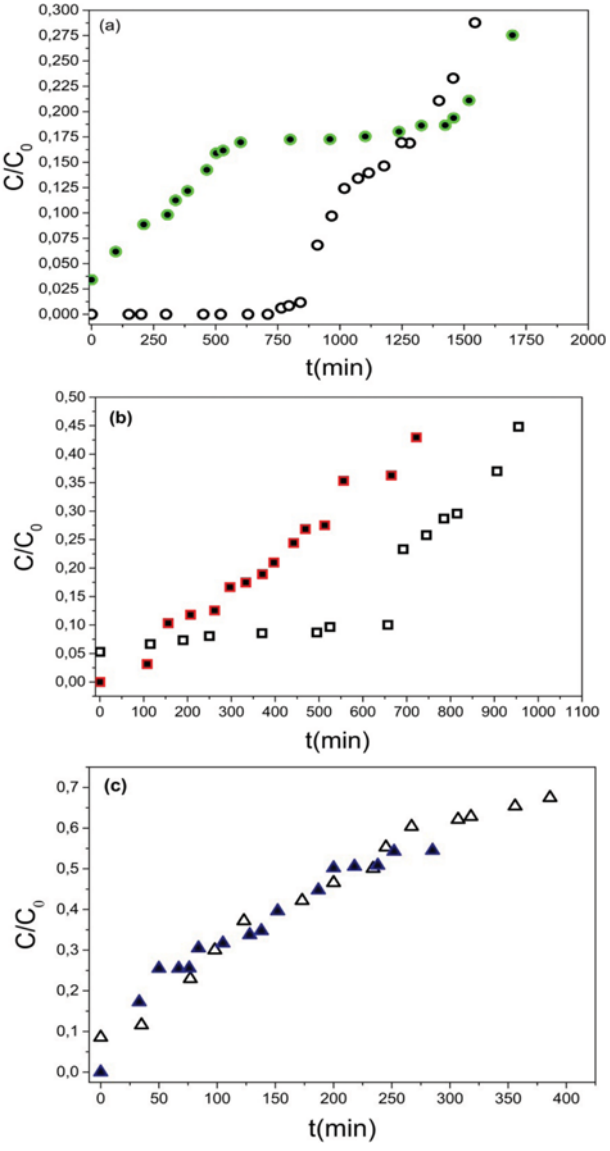

Fig. 6. Breakthrough curves for MB column adsorption before and after regeneration on (a) IAS, (b) Sawdust and (c) SMW. First adsorption cycle (empty symbol), second cycle after regeneration (full symbol).

CONCLUSION

Adsorption of MB in three different adsorbents, IAS, OS and

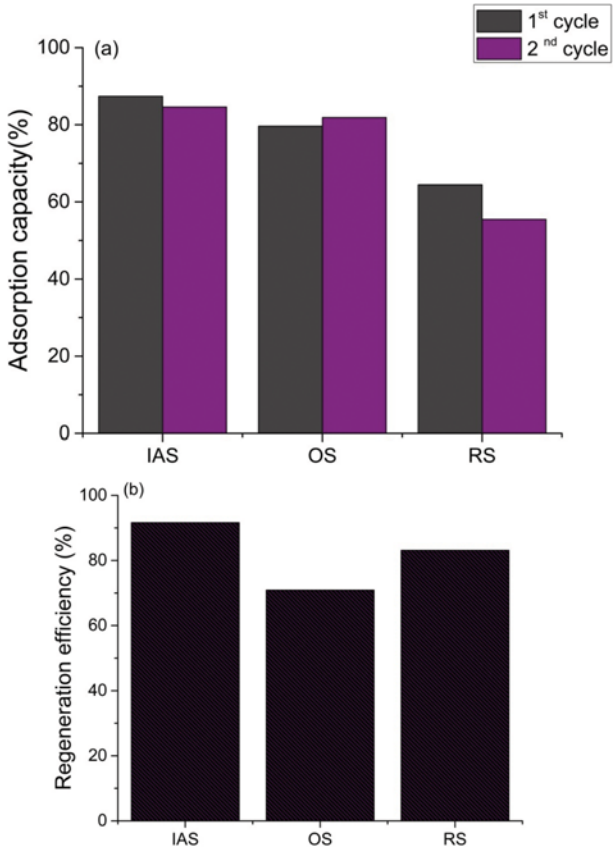

Fig. 7. Comparison column capacity before and after regeneration process and regeneration efficiency for IAS, OS and RS.

RS, was studied in this work in a continuous fixed bed column, and the breakthrough curves and the adsorption parameters were determined. The adsorption capacity follows the order RS<OS< IAS. Also, the RS has the largest mass transfer efficiency due to its high permeability and faster infiltration kinetic. Modified dose-response, Wolborska, Thomas and Yoon Nelson models were used to predict the breakthrough curves obtained from the experimental data. The four used models can be applied in the first part of the breakthrough curves, but the modified dose-response is the better model in the first cycle. Successive adsorption desorption cycle carried out to evaluate the regenerability of the three adsorbents. Adsorption capacity decreases after regeneration of all the adsorbents. IAS and RS represent the higher regenerability of 92% and 83% respectively.

ACKNOWLEDGEMENTS

The authors would like to thank A. Baffoun and A. Moussa for their assistance in the analysis by spectrophotometer.

REFERENCES

1. F. Ramade, Dictionnaire encyclopédique des popullations Ediscience international (2000).
2. V. K. Gupta, D. Mohan, S. Sharma and M. Sharma, *Sep. Sci. Technol.*, **35**(13), 2097 (2000).
3. A. Malik and E. Grohmann, (Eds.), Springer Science and Business Media (2011).
4. K. V. Kumar, V. Ramamurthi and S. Sivanesan, *J. Colloid Interface Sci.*, **284**(1), 14 (2005).
5. P. Manoj Kumar Reddy, S. Mahammadunnisa, B. Ramaraju, B. Sreedhar and C. Subrahmanyam, *Environ. Sci. Pol. Res.*, **20**, 4111 (2013).
6. C. Zhou, Q. Wu, T. Lei and I. I. Negulescu, *Chem. Eng. J.*, **251**, 17 (2014).
7. R. F. Gomes, A. C. de Azevedo, Pereira, E. C. Muniz, A. R. Fajardo and F. H. Rodrigues, *J. Colloid Interface Sci.*, **454**, 200 (2015).
8. W. J. Tseng and R. D. Lin, *J. Colloid Interface Sci.*, **428**, 95 (2014).
9. M. Arshadi, A. R. Faraji and M. Mehravar, *J. Colloid Interface Sci.*, **440**, 91 (2015).
10. G. Z. Kyzas and N. K. Lazaridis, *J. Colloid Interface Sci.*, **331**(1), 32 (2009).
11. S. Sadaf, H. N. Bhatti, S. Nausheen and M. Amin, *J. Taiwan Inst. Chem. Eng.*, **47**, 160 (2015).
12. F. Krika and O. E. F. Benlahbib, *Desalin. Water Treat*, **53**(13), 3711 (2015).
13. M. Shabandokht, E. Binaeian and H. A. Tayebi, *Desalin. Water Treatment*, 1 (2016).
14. M. A. Tahir, H. N. Bhatti and M. Iqbal, *J. Environ. Chem. Eng.*, **4**(2), 2431 (2016).
15. A. Aguedach, S. Brosillon, J. Morvan and E. K. Lhadi, *Appl. Catal. B: Environ.*, **57**(1), 55 (2005).
16. M. Ghaedi, A. G. Nasab, S. Khodadoust, M. Rajabi and S. Azizian, *J. Indust. Eng. Chem.*, **20**(4), 2317 (2014).
17. L. Cottet, C. A. P. Almeida, N. Naidek, M. F. Viante, M. C. Lopes and N. A. Debacher, *Appl. Clay Sci.*, **95**, 25 (2014).
18. C. Li, H. Zhong, S. Wang, J. Xue and Z. Zhang, *J. Indust. Eng. Chem.*, **23**, 344 (2015).
19. M. A. A. Zaini, M. Zakaria, S. M. Setapar and M. A. Che-Yunus, *J. Environ. Chem. Eng.*, **1**(4), 1091 (2013).
20. F. Bouaziz, M. Koubaa, F. Kallel, F. Chaari, D. Driss, R. E. Ghorbel and S. E. Chaabouni, *Ind. Crop. Prod.*, **74**, 903 (2015).
21. R. Subramaniam and S. K. Ponnusamy, *Water Res. Indust.*, **11**, 64 (2015).
22. F. Banat, S. Al-Asheh, R. Al-Ahmad and F. Bni-Khalid, *Bioresour. Technol.*, **98**(16), 3017 (2007).
23. H. Benaissa, *J. Taibah University for Sci.*, **4**, 31 (2010).
24. A. Ahmad, M. Rafatullah, O. Sulaiman, M. H. Ibrahim and R. Hashim, *J. Hazard. Mater.*, **170**(1), 357 (2009).
25. H. Hannachi, M. Msallem, S. B. Elhadj and M. El Gazzah, *C. R. Biol.*, **330**(2), 135 (2007).
26. A. B. Albadarin and C. Mangwandi, *J. Environ. Manage.*, **164**, 86 (2015).
27. H. Deveci and E. Pehlivan, 301 (2010).
28. W. Kaminski, E. Tomczak and S. Kuberski, *Global J. Adv. Pure Appl. Sci.*, 1 (2013).
29. F. D. Ardejani, K. Badii, N. Y. Limaee, S. Z. Shafaei and A. R. Mirhabibi, *J. Hazard. Mater.*, **151**(2), 730 (2008).
30. M. Kandah, *Chem. Eng. J.*, **84**(3), 543 (2001).
31. J. L. Sotelo, G. Ovejero, A. Rodríguez, S. Álvarez and J. García, *Chem. Eng. J.*, **228**, 102 (2013).
32. E. D. Woumfo, J. M Siéwé and D. Njopwouo, *J. Environ. Manage.*, **151**, 450 (2015).
33. K. K. Choy, D. C. Ko, C. W. Cheung, J. F. Porter and G. McKay, *J. Colloid Interface Sci.*, **271**(2), 284 (2004).
34. C. J. Geankoplis, Transport Process and Unit Operations, PTR Prentice Hall, New York (1993).
35. K. Naddafi, R. Nabizadeh, R. Saeedi, A. H. Mahvi, F. Vaezi, K. Yaghmaeian, A. Ghasri and S. Nazmara, *J. Hazard. Mater.*, **147**(3), 785 (2007).
36. Y. H. Yoon and J. H. Nelson, *The American Industrial Hygiene Association J.*, **45**(8), 509 (1984).
37. A. Wolborska, *Water Res.*, **23**(1), 85 (1989).
38. R. Han, Y. Wang, X. Zhao, Y. Wang, F. Xie, J. Cheng and M. Tang, *Desalination*, **245**(1), 284 (2009).